PHYSICAL REVIEW B **74**, 121404(R) (2006)

Subsurface structure of epitaxial rare-earth silicides imaged by STM

C. Rogero,* J. A. Martín-Gago, and J. I. Cerdá
Instituto de Ciencia de Materiales de Madrid CSIC, 28049 Madrid, Spain
(Received 1 March 2006; revised manuscript received 27 June 2006; published 21 September 2006)

We combine scanning tunneling microscopy (STM) images, density functional theory total energy calculations, and STM simulations to conclusively determine the surface structure of the $Y_3Si_5(0001)$ silicide epitaxially grown on Si(111). We observe, for the same sample, two different types of atomic resolution images exhibiting either *p*3*m* or *p*6 symmetry, in analogy with previous works on similar rare-earth silicide surfaces. We elucidate the long-standing controversy regarding the interpretation of these images by showing that they are mainly related to the registry of the surfacemost Si bilayer with respect to the Si vacancy network located two layers below the surface and, therefore, to the existence of two different buried structural domains. Our results demonstrate an unsual STM depth sensitivity—up to 5 Å—for metallic systems.

DOI: 10.1103/PhysRevB.74.121404 PACS number(s): 68.55.Ln, 68.37.Ef, 68.43.Bc

The scanning tunneling microscope (STM) depth sensitivity—i.e., its ability to image buried defects—strongly depends on the system under study. For semiconductor surfaces, and due to the weak screening, impurities located even down to the third layer are well resolved in the images.[1] In the case of metallic surfaces, where the screening is more efficient, one would expect a strong decay of the defect signal with its normal distance to the surface. Nonetheless, there exist several works reporting STM images where defects buried under a metallic surface could be imaged, such as interstitial impurity light atoms at the Pd(111) surface[2] or transition metal atoms buried under noble metal surfaces.[3] A deeply buried two-dimensional (2D) ordered material may also be imaged via the development of stationary waves between the surface and the material.[3,4] Furthermore, the ascription of a specific feature in the STM image to a buried defect is not generally a trivial task and has led to many controversies when trying to determine structural models.[5] In this paper we apply the combination of experimental with simulated atomic resolution STM images for solving a structural problem open in the last decade and not addressable by other techniques: understanding the atomic termination of rare-earth silicides epitaxially grown on Si(111). We will take advantage of the depth sensitivity of a STM image to detect buried vacancies below the third layer and show how they determine the final aspect of the STM images.

The family of metallic thin films of heavy rare-earth (RE) silicides ($\mathcal{R}$=Er,Gd,Dy,Y,etc.) epitaxially grown on Si(111) substrates present very similar atomic and electronic structures.[6,7] They have been broadly studied in recent years because of their appealing properties: unusually low values of the Schottky barrier height [0.3 eV for *n*-type Si (Ref. 8)], a small lattice mismatch (e.g., 0.0% for Y, −1.2% for Er, and 0.83% for Gd silicides),[6] and an abrupt interface. The bulk structure of the RE silicides has been well described from the beginning of the 1990s;[9] they exhibit an AlB_2-type atomic structure, consisting of a hexagonal layered arrangement in which Si and RE planes alternate with each other. In this configuration the Si-Si nearest-neighbor distance is smaller than in the diamond bulk structure (2.2 and 2.35 Å, respectively), leading to a compressive strain. To release the strain, an ordered network of Si vacancies is formed in the Si planes. These Si vacancies induce a relaxation of the surrounding atoms, leading to a Th_3Pd_5 structure and to a $\mathcal{R}Si_{1.7}$ stoichiometry.[10,11] As a result of the periodic arrangement of the vacancies, a $(\sqrt{3}\times\sqrt{3})R30^\circ$ pattern appears in low- and high-energy electron diffraction (LEED and HEED).[7,12,13]

However, and in spite of their technological relevance, the surface structure of the RE silicides is still an open issue. Although it is well accepted that these surfaces are terminated in a bulklike Si bilayer without vacancies,[14] two different structural models have been proposed based on two independent STM studies on the $ErSi_{1.7}$ surface epitaxially grown on Si(111). Roge *et al.* found a hexagonal arrangement of protrusions (*p*6 symmetry) in their STM images,[15] whereas Martín-Gago *et al.* observed a triangular grouping of the protrusions with a *p*3*m* symmetry.[16] Both groups interpreted the protrusions in their images as arising from the upper Si atoms (Si_{up}) in the bilayer but, in order to explain the observed symmetries, they arrived at different registries for the bilayer with respect to the Si vacancies at the third layer. Roge *et al.* concluded that one of the three Si_{up} within the $(\sqrt{3}\times\sqrt{3})R30^\circ$ cell was located on top of a vacancy (Si^v_{up}) with an outward relaxation rendering this atom brighter than the other two Si_{up} (*p*6 model in Fig. 1).[15] On the other hand, Martín-Gago *et al.* assumed it was a lower Si atom in the bilayer, (Si^v_{down}), the one in registry with the vacancies, and invoked lateral relaxations of the three Si_{up} atoms toward the Si^v_{down} in order to account for the threefold symmetry[16] (*p*3*m* model in Fig. 1).

Subsequent work on these surfaces pointed toward the *p*3*m* model. The *ab initio* calculations of Magaud *et al.* found it more stable than the *p*6 model although the total energies for both were very similar.[11] In a LEED study Rogero *et al.* attained a good agreement with experiment for the *p*3*m* case.[12] On the other hand, Duverger *et al.*[17] were able to reproduce theoretically the *p*6-type images, although hardly any reference was made to the *p*3*m* phase.

In this Rapid Communication we reconcile the two models by presenting STM images where both the *p*3*m* and *p*6 phases coexist. We have additionally performed *ab initio* density functional theory (DFT) calculations and STM simulations in order to confirm the correspondence between the experimental images and the two structural phases. It turns out that the symmetry apparent in the images is solely determined by the relative registry of the Si_{up} atoms with respect

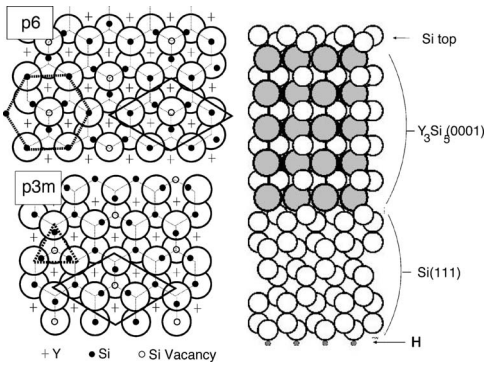

FIG. 1. Left: Top view for the $p6$ and $p3m$ models. Large open white circles correspond to the top Si bilayer. Atoms corresponding to the Y_3Si_5 layers are indicated by small symbols following the legend at the bottom of the figure. Thick solid line, the $(\sqrt{3}\times\sqrt{3})R30^\circ$ cell; thin dotted lines, the buried Si network; thick dashed lines, the observed symmetries in the STM images, hexagons (triangles) for the $p6$ ($p3m$) model. The displacement of the buried Si atoms toward the vacancy is not drawn to scale. Right: side view of the slabs used for the DFT calculations of the $(\sqrt{3}\times\sqrt{3})R30^\circ$ yttrium silicide epitaxially grown on Si(111).

to the buried Si vacancy network located two layers below. Surprisingly, we find that atomic relaxations hardly have any impact on the final aspect of the images. Instead, the two symmetries arise from the propagation of the electronic structure at the third (vacancy) layer toward the surfacemost Si bilayer.

Growth and characterization experiments were carried out *in situ*, in an ultrahigh-vacuum system at room temperature. Our experimental chamber is equipped with a LEED optics, a cylindrical mirror analyzer for Auger electron spectroscopy, and a room-temperature STM. The base pressure was in the low 10^{-10} mbar range, rising to 2×10^{-9} mbar during the evaporation. Y silicides were grown on n-type Si(111) wafers. Their preparation procedure is explained elsewhere.[18] Basically, Y films deposited on Si(111) were annealed at 420 °C for 5 min, resulting in an epitaxially grown silicide, characterized by a sharp $(\sqrt{3}\times\sqrt{3})R30^\circ$ LEED pattern. The film thickness ranged from 5 to 10 monolayers, thus ensuring bulklike behavior for the silicide film.[19]

Figures 2(a) and 2(b) show two types of experimental atomic resolution STM images acquired for the yttrium silicide surface. Figure 2(a) shows a slightly less bright spot surrounded by six brighter features in a hexagonal arrangement with an overall $p6$ symmetry, while Fig. 2(b) exhibits a $p3m$ symmetry due to the triangular grouping of the bright features. These images are in close correspondence with the results that Martín-Gago *et al.* and Roge *et al.* observed, independently, for erbium silicide. The striking point is that both images were acquired on the same sample, in contrast with the aforementioned works, where only one type of image was observed for a given sample. After a detailed analysis of the STM data we have been even able to find areas where both symmetries are simultaneously imaged, as shown in Figs. 4(a) and 4(b) below. Stripes exhibiting $p3m$ or $p6$ patterns can be clearly seen in the image, with boundaries running along the $[\bar{1}2\bar{1}]$ direction. A topographic line scan

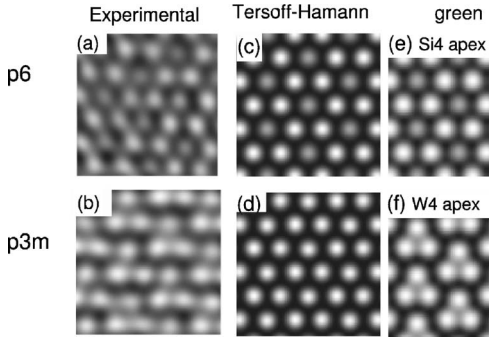

FIG. 2. 2×2 nm^2 STM images for the surface of the yttrium silicide. (a), (b) Experimental topographic images exhibiting $p6$ and $p3m$ symmetries, respectively. Tunneling conditions: $I=1$ nA, $V=-50$ mV. (c), (d) Tersoff-Hamann images evaluated 3 Å above the surface for the $p6$ and $p3m$ models, respectively. (e), (f) theoretical topographic images ($I=1$ nA) calculated with a tip (GREEN calculation). All theoretical images (c)–(f) are calculated for a bias $V=-200$ mV (occupied states).

(not shown) reveals that the surface presents an atomically flat Si bilayer termination even across the domain boundaries, so that there is no step edge separating each domain. This image readily excludes any tip changes as the reason for the existence of the two symmetries but, rather, it is a clear indication that each type of symmetry can be ascribed to a different structural phase.

In order to confirm this picture, we have carried out total energy DFT calculations to deduce the atomic arrangement of both proposed models and compare their energetics. The calculations where performed with the SIESTA code[20] within the local density approximation.[21] The pseudopotentials and the SIESTA specific parameters were tested for several bulk phases: Si diamond, YSi_2 (AlB_2 phase),[22] and Y_3Si_5 (Th_3Pd_5 phase), obtaining in all cases good agreement with previous theoretical work.[11]

To simulate the silicide thin film grown on a Si(111) surface we considered the $(\sqrt{3}\times\sqrt{3})R30^\circ$ 2D slab depicted in Fig. 1. All Si vacancies in the Y_3Si_5 film are assumed to be in registry whereas, following all previous works, the topmost Si bilayer is rotated 180° about the normal with respect to the bulk Si(111). The two possible registries for this bilayer are Si_{up} on top of the vacancy (or $p6$ model) and Si_{down} on top of the vacancy (or $p3$ model). Recall, however, that the overall symmetry for both cases is $p3m$.

Our total energy calculations are basically coincident with the results of Magaud.[11] The $p3m$ model turns out to be marginally more stable than the $p6$ model by just 37 meV. The optimized geometry for the former model shows close agreement with that deduced from a recent LEED analysis.[12] Basically, the Si^v_{down} atom presents a vertical relaxation ($\approx$0.15 Å), while no lateral relaxations were found for any of the surface Si atoms; all of them occupy the ideal hexagonal positions forming, in a top view, a nondistorted hexagon. For the $p6$ model we also found no substantial lateral or vertical relaxations of the Si atoms at the surface bilayer. Therefore, neither the small vertical relaxation in the $p6$ model nor the lateral relaxation in the $p3m$ phase previously proposed from the STM images can be identified in the optimized structures.[15,16]

The fact that the two models essentially share the same unrelaxed structure for the top Si bilayer and the next Y plane is striking. It discards any topographic effects as the source of the observed patterns but, instead, it is a clear indication that the registry of the vacancy network with respect to the top bilayer must play a crucial role. However, how can the STM detect such deep vacancies, given the metallicity of the film?

STM images simulated under the Tersoff-Haman[23] (TH) approximation are displayed in Figs. 2(c) and 2(d) for the $p6$ and $p3m$ models, respectively. Both images exhibit a sixfold symmetry, with protrusions centered on top of the Si_{up} atoms. Figure 2(c) shows close resemblance with the experimental $p6$ image [Fig. 2(a)] with the Si^{v}_{up} appearing dimmer than the surrounding Si_{up} atoms. In accordance with the experiment and previous theoretical calculations for Er_3Si_5,[17] the contrast at the Si^{v}_{up} site was found to vary with the energy window (bias), appearing either brighter or dimmer than at the rest of Si_{up} sites. In the image for the $p3m$ model [Fig. 2(d)] all Si_{up} sites are equally bright, but no triangular grouping among them is visible. These results demonstrate that the symmetry of the electronic structure at the Si_{up} atoms is dictated by their relative registry with respect to the vacancy array at the third layer or, in other words, the vacancy is not fully screened. However, the failure in reproducing the $p3m$ images points out the need to include tip effects in the simulations in order to ensure a correct understanding of the experiments.

To address this issue we have performed more elaborate STM image simulations beyond the TH approach employing the GREEN code.[24,25] The sample is modeled as a semi-infinite stack of 2D layers after replacing the hydrogenated Si bilayer at the bottom of Fig. 1 by bulk Si(111). The tip is also described as a semi-infinite W block [111] oriented, with an isolated—nonperiodic—four-atom tetrahedron stacked at its bottom in order to mimic the tip apex. We have considered two different tip terminations: a W apex (clean tip) and a Si apex (contaminated tip), which could be a standard situation when scanning this type of material. The Hamiltonian of the entire system is described by the extended Hückel theory[26] (EHT) level, with the associated parameters optimized after fitting the EHT electronic structure to the DFT-derived one. The fits were carried out independently for the tip and the sample surface. The elastic tunneling current is then obtained from the Landauer formula via Green's function matching techniques.[25]

We calculated sets of topographic maps for both models and both tips covering a wide range of bias voltages. All simulated images for the $p6$ model are similar to the TH results, displaying a sixfold symmetry with protrusions centered at the positions of the Si_{up} atoms. The brightness of the signal at the Si^{v}_{up} sites, with respect to the other Si_{up} atoms, was also found to vary with the applied bias.[17] Figure 2(e) is an example calculated with a Si4 tip apex. On the other hand, the images corresponding to the $p3m$ model hardly changed with bias and always displayed a $p3m$ symmetry. The W4 tip provides this time excellent agreement with the experiment, as shown in Fig. 2(f). The Si4 tip , on the other hand, leads to somewhat different images (not shown), but which have also been found experimentally. In all cases, the calculated corrugations ($\leq$0.2 Å) are within the range of the measured ones.

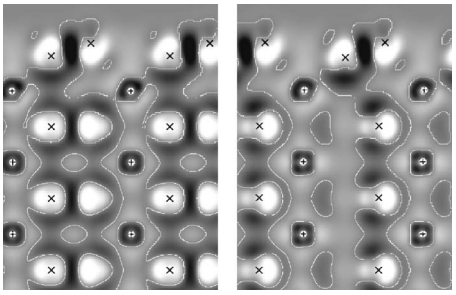

FIG. 3. Charge density difference, defined as the difference between the total CD and the superposition of the atomic densities, for the $p3m$ model. Right (left) panel corresponds to a plane perpendicular to the surface containing (not containing) the vacancy. Both planes contain a Si_{up} and a Si_{down} atom per cell. Solid white line indicates the CDD zero level, while darker (lighter) gray areas correspond to charge accumulation (loss) regions. Atomic labeling is ×, Si atoms; +, Y atoms.

An atomic orbital decomposition of the tunneling current when the tip is on top of each of the maxima in Figs. 2(e) and 2(f) reveals that the dominant contribution comes in all cases from the Si_{up} p_z orbitals—and to a lesser extent the $d_{3r^2-z^2}$—located below the apex. For the $p6$ model the density of states projected (PDOS) onto the Si^{v}_{up} p_z orbital differs from the rest of the Si_{up} atoms, thus yielding different tunneling currents and, hence, the sixfold pattern centered at the Si^{v}_{up}.[17] The picture for the $p3m$ model is somewhat different; here, all Si_{up} atoms are symmetry equivalent and show up in the images equally brightly. This time, the differences in the PDOS between the Si^{v}_{down} and the rest of the Si_{down} atoms are small and cannot be resolved either in the TH image [Fig. 2(d)] or if the Si4 tip is employed, mainly due to the exponential wave function decay. The W4 tip, on the other hand, is capable of detecting this difference due to the larger extent of its s and p orbitals, yielding an enhanced current when the apex is on top of the Si^{v}_{down}(center of the triangles) which leads to the triangular grouping. We have checked that such an enhancement results from a subtle balance between the contribution arising from the Si_{down} under the apex (smaller for the Si^{v}_{down} case) and that arising from the surrounding Si_{up} atoms (larger for the Si^{v}_{down} case). We may conclude that the STM is able to detect the buried vacancies by probing changes induced in the PDOS at the surface Si bilayer. The unexpected fact that the vacancies are not fully screened can be rationalized by recalling the covalent bonding between the Si p and the localized Y d states,[22] which can be clearly appreciated in the charge density difference (CDD) maps displayed in Fig. 3. The presence of the vacancy clearly alters the bonding between the Si_{down} atoms and the first Y plane. Therefore, it is the nature of the bonding at the surface, and not its metallicity, that determines the STM depth sensitivity.

Finally, we address the imaging of buried domain boundaries such as those detected experimentally in Fig. 4(a). To this end we have considered the model depicted in Fig. 4(c); starting from the $p3m$ phase we introduce one defect out of every three in the vacancy array with an overall $c(5\times2)$ periodicity, so that the phase boundaries run along the $[\bar{1}2\bar{1}]$

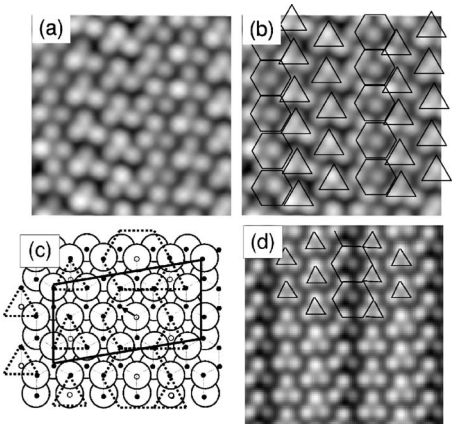

FIG. 4. (a) 10×10 nm^2 STM image where the $p3m$ and $p6$ patterns are simultaneously imaged. Tunneling parameters: $V=-900$ mV and $I=0.8$ nA. (b) Same as (a) but with the hexagons and triangles drawn on top corresponding to the $p6$ and $p3m$ patterns, respectively. (c) Top view of the defect model described in the text. The $c(5\times2)$ cell is indicated by the thick solid line, while the expected triangles and hexagons are highlighted by the thick dashed lines. Symbols for atoms are the same as in Fig. 1. The displaced Si atom at the Y_3Si_5 layer is indicated by a small arrow. (d) Calculated STM topographic image for the geometry depicted in (c) employing a W4 tip apex ($I=1$ nA, $V=-300$ mV).

direction. The defects are created by filling a vacancy with an adjacent Si atom located under a Si_{up}, thus creating a new vacancy below this Si_{up} atom. As a result, the new cell contains two vacancies located below Si_{down} atoms ($p3m$ phase) and a third vacancy below a Si_{up} atom ($p6$ phase). Given the large cell size we did not attempt a DFT calculation for this model, but simply used a guessed geometry for the underlying yttrium silicide film. The STM simulation for this cell, shown in Fig. 4(d), retrieves the most salient experimental features of Fig. 4(a): coexistence of triangles and hexagons with the Si_{up} at its center appearing dimmer. This result fully corroborates one of the main conclusions of this work: the aspect of the STM images is determined by the registry of the Si_{up} atoms with respect to the Si vacancies in the buried yttrium silicide film.

Summarizing, via the combination of STM images and *ab initio* calculations we have been able to identify buried vacancies and domain boundaries at the yttrium silicide surface. Indeed, it is the registry of these vacancies with respect to the almost ideal topmost Si bilayer that determines the symmetry of the STM images, thus allowing us to reconcile the two structural models previously proposed for the RE silicides. Our results show that the STM depth sensitivity may reach down to the third layer at a metallic surface, something hardly accesible by other experimental techniques.

This work has been financially supported by the Spanish DGICyT under Contracts No. MAT2005-3866 and No. MAT2004-05348.

*Electronic address: rogerobc@inta.es

[1] Ph. Ebert, Surf. Sci. Rep. **33**, 121 (1999).
[2] M. K. Rose, A. Borg, T. Mitsui, D. F. Ogletree, and M. Salmeron, J. Chem. Phys. **115**, 10927 (2001).
[3] S. Heinze, R. Abt, S. Blügel, G. Gilarowski, and H. Niehus, Phys. Rev. Lett. **83**, 4808 (1999).
[4] I. B. Altfelder, D. M. Chen, and K. A. Matveev, Phys. Rev. Lett. **80**, 4895 (1998).
[5] H. Kim, W. Kim, G. Lee, and J.-Y. Ko, Phys. Rev. Lett. **94**, 076102 (2005); T. Kubo and H. Nozoye, *ibid.* **94**, 076102 (2005); J. D. Fuhr, A. Saúl, and J. O. Sofo, *ibid.* **92**, 026802 (2004).
[6] R. Baptist, A. Pellissier, and G. Chauvet, Solid State Commun. **68**, 555 (1988).
[7] M. Lohmeier, W. J. Huisman, E. Vlieg, A. Nishiyama, C. L. Nicklin, and T. S. Turner, Surf. Sci. **345**, 247 (1996).
[8] S. Vandré, C. Preinesberger, W. Busse, and M. Dähne, Appl. Surf. Sci. **78**, 2012 (2001).
[9] D. B. B. Lollman, T. A. Nguyen Tan, and J. Y. Veuillen, Surf. Sci. **269-270**, 959 (1992).
[10] A. Iandelli, A. Palenzona, and G. L. Olcese, J. Less-Common Met. **64**, 213 (1979); J. A. Knapp and S. T. Picraux, Appl. Phys. Lett. **48**, 466 (1986).
[11] L. Magaud, G. Kresse, A. Pasturel, and J. Hafner, Phys. Rev. B **55**, 13479 (1997).
[12] C. Rogero, J. A. Martín-Gago, and P. L. de Andrés, Phys. Rev. B **71**, 165306 (2005).
[13] J. Y. Duboz, P. A. Badoz, A. Perio, J. C. Oberlin, F. Arnaud d'Avinaya, Y. Campideli, and J. A. Chroboczek, Appl. Surf. Sci. **38**, 171 (1989).
[14] P. Paki, U. Kafader, P. Wetzel, C. Pirri, J. C. Peruchetti, D. Bolmont, and G. Gewinner, Phys. Rev. B **45**, 8490 (1992).
[15] T. P. Roge, F. Palmino, C. Savall, J. C. Labrune, P. Wetzel, C. Pirri, and G. Gewinner, Phys. Rev. B **51**, 10998 (1995); T. P. Roge, F. Palmino, C. Savall, J. C. Labrune, and C. Pirri, Surf. Sci. **383**, 350 (1997).
[16] J. A. Martín-Gago, J. M. Gómez-Rodríguez, and J. Y. Veuillen, Surf. Sci. **366**, 491 (1996); J. A. Martín-Gago, J. M. Gómez-Rodríguez, and J. Y. Veuillen, Phys. Rev. B **55**, 5136 (1997).
[17] E. Duverger, F. Palmino, E. Ehret, and J.-C. Labrune, Surf. Sci. **595**, 40 (2005).
[18] C. Rogero, C. Polop, J. L. Sacedón, and J. A. Martín-Gago, Surf. Interface Anal. **36**, 1195 (2004).
[19] J. Y. Veuillen, T. A. Nguyen Tan, and D. B. B. Lollman, Surf. Sci. **293**, 86 (1993).
[20] J. M. Soler, E. Artacho, J. D. Gale, A. García, J. Junquera, P. Ordejón, and D. Sánchez-Portal, J. Phys.: Condens. Matter **14**, 2745 (2002).
[21] D. M. Ceperley and B. J. Alder, Phys. Rev. Lett. **45**, 566 (1980).
[22] C. Rogero, C. Koitzsch, M. E. González, P. Aebi, J. Cerdá, and J. A. Martín-Gago, Phys. Rev. B **69**, 045312 (2004).
[23] J. Tersoff and D. R. Hamann, Phys. Rev. B **31**, 805 (1985).
[24] J. Cerdá, M. A. Van Hove, P. Sautet, and M. Salmeron, Phys. Rev. B **56**, 15885 (1997).
[25] www.icmm.csic.es/jcerda
[26] J. Cerdá and F. Soria, Phys. Rev. B **61**, 7965 (2000).